Published in final edited form as:
Structure. 2007 October ; 15(10): 1272–1284. doi:10.1016/j.str.2007.08.010.

A Conformational Transition State Accompanies Tryptophan Activation by *B. stearothermophilus* Tryptophanyl-tRNA Synthetase

Maryna Kapustina[1], **Violetta Weinreb**[2], **Li Li**[2], **Brian Kuhlman**[2], and **Charles W. Carter Jr.**[2,¶]

1 *Department of Cell Biology, University of North Carolina at Chapel Hill, Chapel Hill, NC. 27599-7260*

2 *Department of Biochemistry and Biophysics, University of North Carolina at Chapel Hill, Chapel Hill, NC. 27599-7260*

SUMMARY

B. stearothermophilus tryptophanyl-tRNA synthetase catalysis proceeds via high-energy protein conformations. Unliganded MD trajectories of the Pre-Transition-state complex with Mg^{2+}•ATP and the (post) transition-state analog complex with adenosine tetraphosphate relax rapidly in opposite directions, the former *regressing*, the latter *progressing* along the structural reaction coordinate. The two crystal structures (RMSD 0.7 Å) therefore lie on opposite sides of a conformational free energy maximum as the chemical transition state forms. SNAPP analysis illustrates the complexity of the associated long-range conformational coupling. Switching interactions in four non-polar core regions are locally isoenergetic throughout the transition. Different configurations, however, propagate their effects to unfavorable, longer-range interactions at the molecular surface. Designed mutation shows that switching interactions enhance the rate, perhaps by destabilizing the ground state immediately before the transition state and limiting non-productive diffusion before and after the chemical transition state, thereby reducing the activation entropy. This paradigm may apply broadly to energy-transducing enzymes.

Keywords

Molecular Dynamics; Induced fit; domain motion; transition-state stabilization; Delaunay Tessellation; SNAPP analysis; molecular switching; Multi-mutant cycles

Introduction

Class Ic tyrosyl- and tryptophanyl-tRNA synthetases catalyze amino acid activation largely by using the binding energy available in the adenosine and PPi moieties of ATP for transition state stabilization (Fersht, 1987; Fersht et al., 1988; First and Fersht, 1995; Kapustina and Carter, 2006; Retailleau et al., 2003; Retailleau et al., 2007). Although this reasonable idea has substantial experimental support, there is no clear structural model of how changes in a protein's structure actually convert binding free energy into rate enhancement.

¶Corresponding author: Tel: 919 966-3263, Fax: 919 966-2852, Email: E-mail: carter@med.unc.edu.

Structural studies on GlnRS (Bullock et al., 2002; Sherlin and Perona, 2003), GluRS (Sekine et al., 2003a; Sekine et al., 2003b), TyrRS (Cusack et al., 2002), ArgRS (Delagoutte et al., 2000; Sekine et al., 2001), and TrpRS (Doublie et al., 1995; Ilyin et al., 2000; Retailleau et al., 2003; Retailleau et al., 2001), all show catalytically relevant relative movement of their Rossmann fold (RF) and anticodon-binding (ABD) domains. *B. stearothermophilus* tryptophanyl-tRNA synthetase, TrpRS, as an extreme case, may accentuate functionally homologous structural variation that is more subtle for related enzymes. The extensive TrpRS structural reaction profile is thus a substantive source for missing details.

TrpRS uses three-state behavior to implement the three canonical stages of enzymatic catalysis (Figures 1 and 3A). Induced fit, driven by binding both tryptophan and ATP assembles the active site by closing and twisting the ABD relative to the RF. The resulting pre-transition-state (PreTS) conformation, represented by 1M83, an off-path ATP complex that accounts for substrate inhibition observed at high [ATP], and 1MAU, an arguably on-path complex with both tryptophanamide and ATP, was previously hypothesized for TyrRS (Fersht, 1987) as a distinct, high-energy state in the absence of ligands. Studies of TrpRS have now defined its structure (Retailleau et al., 2003) and verified its high relative conformational free energy (Retailleau et al., 2007). The catalytic step involves untwisting the ABD domain, which relocates the PPi leaving group to form a third conformation that remains closed and retains Trp-5′AMP (Products), (Doublie et al., 1995; Retailleau et al., 2001). Studies of crystal growth and an incomplete low-resolution structure of a tRNA complex imply that tRNA aminoacylation and, implicitly, product release, re-opens the monomer (Carter, 2005). In keeping with the behavior of other free-energy transducing enzyme systems (Carter et al., 2002), these domain motions are consistent with the progression of high-energy bonds linking the adenosine moiety first to the PPi leaving group, then to tryptophan, and finally from tryptophan to $tRNA^{Trp}$.

The TrpRS conformational free energy profile was clarified by MD simulations of all three TrpRS conformational states (Figure 1 in (Kapustina and Carter, 2006; Kapustina et al., 2006)). Open and Products trajectories are stable, even without bound ligands. PreTS trajectories are stable if both substrates are present. Without ligands, the structure reverts rapidly to the open conformation, and can be stabilized only by restraining the relative domain orientations. In contrast to the regression of unliganded PreTS trajectories along the reaction coordinate, unstable trajectories containing ATP all *progress*, untwisting toward the Products conformation (Figure 1B). Thus, bound nucleotide switches the direction along which the structural instability is manifested, consistent with the proximity of the PreTS state to a conformational free-energy maximum.

Unrestrained MD trajectories of the PreTS Mg^{2+}•ATP complex in PDB ID 1M83, with virtual mutations and restraining potentials demonstrated that stabilizing the high twist requires competition between Mg^{2+}- and lysine-phosphate interactions for the non-bridging oxygen atoms (Kapustina and Carter, 2006). Bound ATP, even with Mg^{2+}, did not stabilize the trajectory unless the Mg^{2+} was restrained to its crystallographic position away from the phosphates, as molecular mechanics force fields do not properly represent the delicate balance of electrostatic forces. This behavior implies an activation of Mg^{2+} during induced fit.

We recently solved the structure of TrpRS complexed to adenosine 5′ tetraphosphate (AQP; (Retailleau et al., 2007)). Insertion of the β-phosphate in AQP allows the adenosine and terminal pyrophosphate to form stronger interactions, respectively, with the ribose binding site and a reconfigured KMSKS loop, mimicking a transition state with dissociative character. AQP binds 200-fold tighter than ATP in both induced fit and steady-state exchange equilibria. The enhanced AQP binding interactions that result from domain untwisting and loop movement provided a detailed structural rationale for previous mutational and pre-steady-state kinetic

results for TyrRS (Fersht, 1987; Fersht et al., 1988; Retailleau et al., 2007). Moreover, parallel thermodynamic cycles provided by ATP and AQP affinities to different TrpRS conformations led to an experimental estimate of +3.0 kcal/mole for the allosteric constant. The free energy "stored" by domain movement is therefore available for transition-state stabilization as suggested, without structural details, by Fersht (Fersht, 1987; First and Fersht, 1995).

Key questions remain. Are there experimental correlates of linkage between TrpRS conformation and Mg^{2+} coordination? Is conformational free energy stored in the twisting or hinge-bending domain motion? Is it recovered during the catalytic untwisting step? What switching interactions impose three-state behavior? How do conformational free energy differences arise from the structures? We address these questions by measuring the effect of Mg^{2+} on TrpRS-ATP affinity and by simulating the bound and unliganded MD trajectories of the recent AQP-bound structure, 2OV4. We show that PreTS and AQP-bound TrpRS structures lie on opposite sides of a conformational free energy maximum, consistent with energy storage and recovery during catalysis. Delaunay tessellation and SNAPP scoring (Carter et al., 2001; Sherman et al., 2004; Tropsha et al., 2003) implicate the high twist angle as the primary source of conformational strain. We identify sidechain packing changes in four discrete "conformational switches" and show that different conformational free energies arise from distributed, long-range interactions developed via molecular switching. Finally, mutation of a switch both reduces k_{cat} and facilitates catalysis by Mn^{2+}, thus establishing coupling between conformational switching and catalytic metal-triphosphate interactions. Our methods and results may apply to a broader class of energy-transducing enzymes.

Results

The TrpRS RF and ABD domains provide the major binding determinants for adenosine and PPi, respectively, and their relative motion is key to catalysis. Of the two conformational angles describing relative motion ((Kapustina and Carter, 2006; Kapustina et al., 2006); Figure 1A), the hinge, α, responds to the nucleoside moiety, irrespective of whether it is covalently linked to PPi or to Trp. Crystal structures saturated with such ligands (Mg^{2+}•ATP, Trp-5′AMP, and its analogs) have closed hinge angles. The twist angle, γ, however, is sensitive to precise interactions with the triphosphate. Calorimetry and MD simulations both implicate coupling between the high conformational twist angle and the bent, catalytically competent PreTS Mg^{2+}-triphosphate configuration.

Stabilizing the twist: ITC titrations and MD simulations ±Mg^{2+}

Isothermal titrations with two TrpRS and ATP concentrations, ± Mg^{2+} ion (Figure 2) show more complicated behavior than those for AQP (Retailleau et al., 2007). Simple binding models cannot be fitted for parameter estimation. However, Mg^{2+} induces a lateral shift of the similar profiles to higher [ATP], implying that Mg^{2+} weakens the TrpRS-ATP interaction by ~0.5–1.0 kcal/mole.

Mg^{2+} also weakens the simulated PreTS state. Trp and ATP, but without Mg^{2+}, lead to the most stable PreTS MD trajectory; both hinge and twist angles remain very close to crystallographic values (Figure 3A). With Mg^{2+}, the mean twist angle falls by 15% ($P<10^{-5}$), without changing the hinge (P=0.57). As there are no protein-Mg^{2+} contacts in any of the TrpRS•ATP complexes, competition for the phosphates weakens phosphate-lysine interactions sufficiently in the PreTS state to account for reduced ATP affinity with Mg^{2+}; the modest magnitude of the calorimetric effect is consistent with observation of lysine-phosphate contacts in PDB IDs 1M83 and 1MAU.

Unliganded AQP complex trajectories progress along the reaction coordinate

MD Trajectories of *unliganded* states reveal conformational energetics of the structural reaction profile. The unliganded PreTS state regresses within 2 ns to one resembling the crystallographic Open conformation (Kapustina and Carter, 2006). Bound ATP with any partial combination of the other stabilizing factors leads invariably to progression toward the Products configuration. The similarity of the latter trajectories to that presumed from the crystal structures to occur during catalysis suggests that bound nucleotide changes the free energy landscape by disfavoring return to the open conformation and favoring the path to the Products conformation.

Here, we describe new ~5 ns simulations initiated from the AQP crystal structure, 2OV4 (Retailleau et al., 2007). Liganded and restrained, unliganded trajectories are stable (Figure 3B). Without the restraining potential, the unliganded AQP structure *progresses* rapidly toward the Products state, despite the absence of bound nucleotide. The bias toward progression, induced into the PreTS state by bound ATP, has become intrinsic to the unliganded structure in the AQP complex.

Cα positions in the PreTS and AQP crystal structures differ by an RMSD of only 0.7 Å, scarcely more than experimental error (Retailleau et al., 2001). Yet without ligands, their MD simulations relax in opposite directions. The possible paths between the two conformations must pass through a free energy maximum for their relaxations to differ so decisively. By definition, TrpRS therefore displays a “conformational” transition state as it binds to the chemical transition state.

SNAPP analysis correlates with stability along the structural reaction path

Commitment of the unliganded PreTS and AQP trajectories to opposite directions provides strong evidence of functional structural differences. Side chain packing between the two states must switch between regression and progression along the catalytic reaction coordinate. Our goal here is to find structural correlates of “conformational switching” and examine its mechanism.

This problem is one for which there is no accepted strategy. Extracting subtle structural insight from details in MD trajectories is difficult at best. We turn instead to the static crystal structures, whose structural redundancy affords the opportunity to apply bioinformatic methods.

Of the available algorithms, Delaunay tessellation has several advantages. First, it provides an unambiguous map of nearest neighbor interactions in a protein by decomposing the three-dimensional structure uniquely into its simplices. The resulting simplification reduces packing details to a level where they can be readily examined. Empirical (Carter et al., 2001) and theoretical (Bandyopadhyay, 2005) studies have shown that simplicial decomposition is also robust to small coordinate errors.

Second, **S**implicial **N**eighborhood **A**nalysis of **P**rotein **P**acking (SNAPP; (Tropsha et al., 2003)) provides a virtual free energy map of packing relations in proteins from the frequency of simplices with the same amino acid composition in the structural database. As three-dimensional Delaunay simplices are always tetrahedra, the ratio of observed to expected frequencies for the 8855 possible quadruplet compositions provides a log-likelihood for each quadruplet, ijkl, $\Lambda_{ijkl} = \log(f_{ijkl}/p_{ijkl})$. Energy-ranked tetrahedra can be clustered. Further, as each side chain participates in different numbers of tetrahedra, the total SNAPP score provides a unique metric for each residue.

As the logarithm of something akin to a virtual equilibrium constant, Λ_{ijkl} correlates with stability measurements made on mutant proteins (Carter et al., 2001). For a series of bacterial

periplasmic binding proteins, the open unliganded crystal structures have higher total SNAPP scores than the closed, liganded species, consistent with their implicit thermodynamic stabilities without bound ligands (Sherman et al., 2004). Encouraged by that precedent, we did a SNAPP analysis of 17 different structures from the TrpRS conformational cycle: open Trp (1MB2) and ATP (1MAW) complexes with six monomers; PreTS complexes with ATP (1M83) and ATP + tryptophanamide (1MAU); AQP complex (2OV4); and Products complexes (1I6K, 1I6L, 1I6M), each with a single monomer in the asymmetric unit.

We evaluated pairwise correlation coefficients between the 326-element residue-by-residue SNAPP profile vectors, to assess statistical significance of structural clustering relative to coordinate errors. Next, to assess the energetic profile, we compared mean total SNAPP scores for statistically distinct clusters. Finally, we used regression analysis to correlate total SNAPP scores with variations in the two internal conformational angles.

Clustering based on profile analysis—Cross-correlation of residue-by-residue SNAPP profiles establishes four, statistically distinct groups of structures (Figure 4A): Open, PreTS, AQP, and Products. Excepting the PreTS-AQP comparison, these differ by more than twice the standard deviation within clusters, and correlation coefficients between these and the remaining structures establish that they, too, differ significantly in their SNAPP profiles (Figure 4A).

Total SNAPP scores and the structural reaction profile—Consistent with the MD trajectories of unliganded PreTS and AQP structures, these two structures have significantly lower total SNAPP potentials than the Open and Products states (Figure 4B). A parabola fitted to the $\Delta SNAPP_{rel}$ values assuming unit intervals between structures passes through a maximum just before the AQP structure. Coincidence of the MD and SNAPP analyses suggests that both capture elements of the conformational destabilization documented by the experimental allosteric constant (Retailleau et al., 2007).

Reduced SNAPP scores result almost entirely from the twist angle—Structural redundancy allows us to ask whether the decreased PreTS and AQP state SNAPP scores arise from hinge closing, from twisting, or from their combination. We fitted the 17 total SNAPP scores as dependent variables to a linear combination of the two internal coordinates. The twist angle alone predicted the SNAPP score with an $R^2 = 0.81$ and a t-test $P_{twist} < 0.0001$. R^2 was unchanged when the hinge angle was added and $P_{hinge} = 0.4$. Thus, the reduced SNAPP scores that correlate with PreTS state destabilization arise almost entirely from packing changes associated with the high twist angle, as proposed (Kapustina and Carter, 2006).

Delaunay tetrahedra rearrange during catalysis

Delaunay tetrahedra can be compared from structure to structure (Figures 5–6) to identify more detailed structural changes from the SNAPP analyses. Alternately, differential ΔSNAPP profiles can be displayed, residue-by-residue (Figure 7). The two comparisons provide complementary localization of significant structural changes.

Long-range interactions: Delaunay simplices that change composition—Tessellation of side chain centroids in the TrpRS monomer produces ~250 tertiary simplices (ie., no participants adjacent in sequence). Considering just the closed structures related to the catalytic step, ie., PreTS, AQP, and Products, ~75% of these simplices do not change, indicating the extent to which the catalytic step approximates rigid-body domain motion. The remaining 25% of the simplices exchange neighbors in one or both structural transitions.

Surprisingly, the dominant contributions to the overall ΔSNAPP values in Figure 4B arise not from high-Λ simplices, but from exchanges among those with negative log-likelihoods (Figure 5). Such quadruplets occur less frequently as nearest neighbors than expected under the null hypothesis and presumably affect protein stability adversely. They border clusters of higher-Λ simplices at the protein surface, especially near the domain interface (Compare Figures 5B and 6B,C).

Switching interactions—A total of 70 Delaunay tetrahedra in TrpRS have SNAPP log likelihood scores, $\Lambda > 0.6$. Turning to these, we find that 57–59 (~85%) are within rigid bodies and do not change as the PreTS structure evolves through the AQP structure to the Products conformation. Six high-Λ Delaunay tetrahedra do change composition between the PreTS and AQP states on either side of the chemical and conformational transition state. These occur in four separate clusters, D1–D4, distributed around the Rossmann fold (Figure 6).

The four cluster centers of mass are distant from the active site and represent long-range interactions between the active site and distal functions (the anticodon binding domain (D2, D4) and the dimer interface (D3)). Their specific rearrangements, tabulated in Figure 6A, have the characteristics of a switch: breaking and reforming similar, but alternate, configurations. All seven PreTS tetrahedra change in the AQP state, which forms new compositions in three of the clusters (D1–D3) and loses D4 (containing M193 from KMSKS) entirely (Figure 6B). Six tetrahedra lost in forming the AQP complex from the PreTS state, including D4, are re-formed in the Products conformation. Cluster D3 gains a tetrahedron in the AQP state that persists in the product state, and so differs between the PreTS and Products States. Curiously, it links the active site to the dimer interface, which is also perturbed in the Products state (unpublished results).

Residue-by-residue ΔSNAPP profiles—Difference profiles comprise a linear map of energetically significant structural perturbations along the sequence. SNAPP scores decrease between Open and PreTS states, and increase between PreTS and Products states (Figure 7A). Changes occur chiefly in groups highlighted in three ellipses corresponding roughly to clusters D1, D2, and D4 in Figure 5: the β-strand and α-helix on either side of the HIGH sequence, a group of residues from the “bearing helix” including L66, and residues surrounding M193 from the KMSKS signature. Similar side chain groupings were previously identified using graph theoretic methods (Ilyin et al., 2000). In particular, F26 and L29 (D1) and Y65 (near D2) were identified as a bearing for domain movement. Cluster D3 makes separate interactions between the tryptophan-binding site, the dimer interface, and the extreme C-terminus. Changes introduced in the AQP state are overlapping, but distinct (Figure 7B). Notably, the vertical reflection symmetry of the profiles close to the HIGH and KMSKS signatures in Figure 7A is broken in the detailed passage through the AQP state.

Mutation of the D1 switch has multiple effects on catalysis

A master switch?—Structural hierarchy in the switching interactions suggests that they may have contributed to catalysis in ancestral class I aaRS. D1 and D4 clusters form entirely from residues within a 130-residue minimal catalytic domain (MCD; (Pham et al., 2006)), suggesting that the MCD may also undergo rudimentary conformational switching related to catalysis. Later addition of the D2 and D3 clusters may have amplified that catalytic effect in full-length TrpRS.

Compositional exchange occurs between three group D1 tetrahedra suggesting that it may function as a “master switch” (Figure 8A,B). D1 lies at the corner of the first α- β- α crossover opposite the HIGH sequence and KMSKS loop, forming links to I4 in the N-terminal β-strand and I140 in the Trp binding site. Three of its side chains (F26, Y33, F37) are aromatic. F26

rearranges significantly relative to F37 during induced fit, switching from F26(face)-to-F37 (edge) packing (Burley and Petsko, 1985) in the open state to the energetically-preferred face-to-face stacking (McGaughey et al., 1998) as the hinge closes to form the closed states (Figure 8A).

As the switching interactions represent packing combinations compatible with TrpRS's multi-state behavior, they are opportunities to use protein design to stabilize each structure along the reaction coordinate (Marvin and Hellinga, 2001; Shimaoka et al., 2000) by mutation. We therefore used the Rosetta Design program to generate stabilizing mutations for each of the three principal conformations along the structural reaction profile. Remarkably, consensus mutations suggested by Rosetta selected each residue in cluster D1 to "hyperstabilize" the PreTS state: I4V, F26L, L29A, Y33F, C35V, F37I, and I140Y.

The F37I/Mn^{2+} multimutant thermodynamic cycle—We have constructed each of these single mutants, and various combinations, including the complete set. Results for the F37I mutation, the first we have studied, are shown in Figure 8C. We used ATP-dependent Michaelis-Menten kinetics to examine the double-variant thermodynamic cycle (Horovitz and Fersht, 1990) consisting of the F37I mutation together with substitution of Mn^{2+} for Mg^{2+} to probe conformational effects on both catalysis and Mg^{2+} coordination. Mn^{2+} reduces the wild type TrpRS k_{cat} nearly one hundred fold (Retailleau et al., 2003), reflecting (undetermined) differences in metal coordination and its catalytic effects.

The F37I mutant exhibits statistically significant main and two-way interaction effects arising from altered switching in the D1 cluster. It elevates the transition state free energy by 1.1 kcal/mole with Mg^{2+}, consistent with stabilization of the PreTS conformation. Unexpectedly, however, this effect is only 0.26 kcal/mole with Mn^{2+}. The Ile substitution at position 37 substantially facilitates catalytic coordination of Mn^{2+}, reducing the adverse effect of metal substitution from 2.52 to 1.68 kcal/mole. The mutation could: (i) reduce the destabilization of the conformational transition state and (ii) flatten the energy barrier between conformations, relaxing the switching. The effect on k_{cat} is readily explained by (i) and the interaction with the divalent metal is consistent with (ii).

Transition state stabilization via long-range interactions

In summary, unliganded MD trajectories initiated from the PreTS and AQP crystal structures (Figure 3B), and the ΔSNAPP profiles (Figure 4B) are consistent only with the existence of a higher-free energy structure between them, extending the original conclusions for TyrRS (Fersht, 1988; Fersht et al., 1988) (Figure 9A). We also implicate a unique Mg^{2+}•ATP configuration in creating this conformational free energy maximum, which occurs along the reaction coordinate close to, if not coincident with the chemical transition state.

Four specific, high-Λ packing interactions change between the PreTS, AQP, and Products structures. Alternate configurations of D1–D4 have nearly the same SNAPP potentials, but are linked to distinct, unfavorable interactions propagating from them in the PreTS and AQP states. These properties are precisely those expected if switching interactions are broken in the conformational transition state. The conformational and chemical transition states are separated schematically in Figure 9B. Four stages are implicated: induced fit and Mg^{2+} activation (I), conformational switching (II), high-affinity transition state binding (III), and relocation of the KMSKS loop and the PPi binding subsite to recover the stored conformational free energy (IV).

Discussion

Transducing enzymes convert irreversible aqueous NTP hydrolysis into an enzyme-bound reaction whose equilibrium constant is close to unity. Doing so transiently stores the ability to do work in unfavorable protein conformations. We describe here how TrpRS implements this paradigm: the chemical transition state is recognized by a high-energy protein conformation. If not stabilized by ligands, this "conformational transition state" decays either backward or forward along the reaction coordinate, the choice depending on switching interactions distributed throughout the molecule. Switches are set either by binding stable ligands resembling preTS or postTS configurations, or by chemical conversion of the NTP substrate during catalysis.

Aminoacyl-tRNA synthetases have not been widely recognized as transducing enzymes, although the fundamental observation that TyrRS proceeds via an ATP-dependent high-energy conformation was postulated nearly two decades ago (Fersht, 1987; Fersht et al., 1988). This work breaks new ground by documenting the conformational free energy maximum, and pinpointing packing interactions that change as the conformational transition state (which must exist for any enzyme that stores chemical free energy) is traversed. We use computational geometry to distinguish between switching and destabilizing interactions, and show SNAPP analysis to be a valuable, high sensitivity probe for discovering and filtering subtle changes. Finally, we illustrate conformational coupling to catalysis by the F37I/Mn^{2+} double variant cycle.

Our results raise four questions about TrpRS catalysis. How simultaneous are the conformational and chemical transition states? Are induced fit free energy changes related to those establishing the catalytic Mg^{2+} configuration? How does the conformational transition state accelerate the catalyzed rate? Can switching itself also contribute to catalysis?

We have argued (Retailleau et al., 2007) that the AQP complex captures structural aspects of the enhanced binding to adenosine and PPi moieties in the transition state for tryptophan activation. Although it captures neither the geometry of the Mg^{2+} ion or the α-phosphate, AQP represents a structural analog for transition state adenosine and PPi binding because the rate-enhancing binding energies are distributed into their binding subsites, far from the scissile bond, as elucidated experimentally for TyrRS (Fersht, 1987; Fersht et al., 1988; First and Fersht, 1993b; First and Fersht, 1995). The following aspects of the AQP complex suggest that the conformational and chemical transition states may be closely correlated:

- **i.** It is nearly within experimental error (0.7 Å RMSD) of the PreTS structure, so structural evolution through the transition state is both structurally and energetically minimal.
- **ii.** Its total SNAPP potential is smallest of all structures along the profile, and packing in D1–D3 is unique, suggesting that it most closely resembles the conformational transition state. As simulation of the unliganded AQP complex progresses along the reaction coordinate, it probably approximates a *post* transition-state conformation.
- **iii.** The ground state active-site structure is disrupted in the AQP complex. Specifically, in the PreTS ATP complex S194 forms a hydrogen bond with K192 and does not interact with the PPi moiety (Retailleau et al., 2007). In the AQP complex, this hydrogen bond is broken and both component residues interact with the PPi leaving group. Loss of the D4 tetrahedron opens the KMSKS loop to improve binding interactions with the PPi leaving group, suggesting proximity to the transition state.
- **iv.** Reformation of the D4 cluster activates the KMSKS loop movement that relocates PPi.

Induced fit brings the two substrates together for reaction. The weakening of ATP binding by Mg^{2+} suggests that it has a more subtle purpose: to activate the divalent metal. Both the bent triphosphate configuration imposed by Mg^{2+} and the weakening of metal-phosphate bonds are important for Mg^{2+} activation. There is curious agreement between the free energy stored during induced fit (3.0 kcal/mole; (Retailleau et al., 2007)) and the potential of mean force estimate (PMF) for the work (Helmholz free energy, ~4.3 kcal; (Kapustina et al., 2006)) required to move the Mg^{2+} ion against the CHARMM force-field to its crystallographic position. The former measures the conformational work done to bring and maintain the lysine ε-NH_2 groups within range of the Mg^{2+}-oriented ATP phosphate oxygen atoms and achieve the correct twist angle. On the other hand, the minimum energy of the CHARMM force field reproduces the shorter Mg^{2+} oxygen distance observed in Mg^{2+}•phosphate coordination structures, so the PMF measures the work exerted to pull the Mg^{2+} sufficiently away from the phosphate groups to allow the lysines to bind. The experimental and computational free energies can therefore be viewed as alternative estimates for the work to achieve the high twist angle of the PreTS state. Thus, because lysine-phosphate and Mg^{2+}-phosphate interactions are coupled, their approximate agreement seems more than coincidental.

Two recent developments implicate conformational effects in the TrpRS catalytic rate enhancement. First, a monomeric 130-residue minimal catalytic domain (MCD) (Pham et al., 2006), roughly twenty percent as large as dimeric TrpRS, is only 4–5 orders of magnitude slower than that of the intact enzyme. The MCD contains a nearly complete active site (missing only K111) but few long-range interactions. Second, the Mg^{2+} ion contributes only 5 of approximately 14 orders of magnitude to the overall rate enhancement of full length TrpRS (Weinreb and Carter, 2007). Rate enhancements of roughly 9 orders of magnitude for full-length TrpRS and perhaps 4–5 orders of magnitude for the MCD are therefore intrinsic to the proteins themselves.

The nature of these intrinsic catalytic contributions remains unresolved. Long-range interactions provided by the additional mass of the full-length enzyme likely contribute significantly to the rate acceleration observed for the contemporary enzyme. At least two strategies could be involved: ground-state destabilization and switching via the conformational transition state.

Mutation of the TyrRS KMSKS loop led First and Fersht to conclude that it prevented formation of a tight ground state ATP complex, while allowing the lysine residues to bind tightly only in the transition state (First and Fersht, 1993a; First and Fersht, 1993b). Our results reinforce this conclusion in detail. The unfavorable induced fit conformational free energy (Retailleau et al., 2003) destabilizes the ground-state interaction with ATP, consistent with the ITC results. The MD simulations and virtual free energy profiles in Figure 4B both also imply ground-state destabilization. Loss and recovery of the D4 cluster; weakening of ATP binding by Mg^{2+}; the Mg^{2+}-lysine electrostatic competition; and the (paradoxically) stronger AQP•TrpRS interaction, in which substituting the β-phosphate group for Mg^{2+} (Retailleau et al., 2007) strengthens interaction with K192 and S194 all imply differential use of KMSKS loop binding energies before, during, and after the transition state. The TrpRS active site coordinates with Mg^{2+} to grasp the ATP transition state elastically, quite literally like a stretched rubber band, whose elasticity is enhanced by the long-range interactions sketched in Figures 4–7.

The impact of the F37I mutation is also consistent with ground state destabilization. Analyses both by Rosetta and by virtual mutagenesis using the MUSE algorithm devised by Cammer (Carter et al., 2001) indicate that the Ile for Phe substitution should stabilize both PreTS and Products conformations relative to the OPEN conformation. The mutant should, therefore, slow the reaction by stabilizing the ground-state, as observed. More extensive characterization of

the designed D1 cluster mutations to determine their effect on the catalytic cycle can open a new experimental window on how long-range interactions promote catalysis.

The thermodynamics of the conformational cycle arise by propagating many effects from the alternate, high-Λ switching interactions in core regions throughout the periphery (Figure 5B). Although perhaps counter-intuitive, this result actually makes sense. Core switching regions are composed of non-polar side chains, all of which participate in high-Λ packing. Exchanging partners among these side chains will likely form approximately equivalent SNAPP potentials in alternate, nearly isoenergetic local minima capable of nucleating conformation changes whose equilibria are determined by numerous propagated effects. This work complements previous work correlating SNAPP scoring of mutations in core, high-Λ tetrahedra with protein stability (Carter et al., 2001) by providing the first evidence that negative-Λ tetrahedra are important for differential protein stability.

Rates of the large conformational changes – induced-fit and product-relocation – are unknown and likely ligand-dependent. Thermodynamic cycles of adenine nucleotide binding (Retailleau et al., 2007) suggest that PreTS TrpRS turns over without relaxing to the Open conformation and that induced-fit is relatively slow. Similar considerations apply to the subsequent untwisting.

In addition to narrowing the gap between ground state and transition state ATP binding, the TrpRS conformational transition state imposes molecular switching between the PreTS and PostTS states. Repacking in two of the six tetrahedra in Figure 7 exchanges one partner for another adjacent in sequence along an alpha helix (V299-L300 for D2 and L134-L135 for D3), characteristic of conformational shear, a slow process, relative to hinge-bending (Krebs et al., 2003). Conformational switching between two quite similar conformations (PreTS and AQP) may nevertheless be more rapid than untwisting to the Products conformation and need not be rate-limiting. Local free energy minima may instead keep the respective active site interactions from changing unless the substrate chemistry changes, that is unless the substrates proceed to or from the transition state. By discretizing the configurational space accessible to the reacting molecules, molecular switching restricts active-site ensembles more precisely to configurations related, respectively, to reactants and products. Thus, they may channel off-path chemical diffusion and enhance the rate by reducing entropy in the neighborhood of the transition state. Combining switching with exergonic relocation of the PPi binding subsite would ensure that once past the conformational transition state, the ensemble would move rapidly to products.

Methods

MD trajectories

Simulations of the PreTS state and its relatives were carried out as previously described (Kapustina and Carter, 2006). Force fields and molecular parameters for AQP were adapted from those used for ATP. Molecular dynamics simulations for TrpRS monomers were performed with the program SIGMA (Mann et al., 2002), using the CHARMM27 force field. Snapshots were saved every 400 fs.

Isothermal titration calorimetry

Isothermal titrations with ATP ± stoichiometric Mg^{2+} Chloride was performed using a Microcal VP-ITC. Titrations were carried out at two different proteins concentrations (60 and 245 μM) using two different ATP concentrations (15 mM and 0.1 M).

SNAPP analysis

Delaunay tessellation and likelihood scoring, were done using the Procam web interface (http://staff.vbi.vt.edu/cammer/procam.html). High (Λ>0.9) likelihood tetrahedra formed by nearest neighbors were extracted from the resulting kinemage files. These were then sorted on Λ, and aligned against one another to identify differences. Residue-by-residue profiles were assembled into column vectors for the purpose of correlation analysis, which was performed using JMP (SAS, 2004).

Mutagenesis

The F37I mutation was constructed using the GeneTailor kit (Invitrogen). The expression plasmid pET11a containing wild type TrpRS was methylated by DNA methylase and used as template for mutagenic PCR. Primers were designed to prime in opposite directions, with a 15–20 nucleotide overlap for efficient circularization. The PCR product was used to transform DH5α *E. coli* cells, and plated on LB plates with ampicillin. The resulting plasmid was sequenced to confirm the successful introduction of the mutation.

Enzyme purification

The F37I mutant was expressed in *E. coli* BL21(DE3)pLysS, with both ampicillin and chloramphenicol, harvested and resuspended in 50 mM Tris, 10% Sucrose, pH 7.5 and rapidly frozen. The cell paste was homogenized with an EmulsiFlex C-5 homogenizer and cleared by centrifugation at 4°C. Ammonium Sulfate to 30% was added to this supernatant, which was heated at 65°C 30 min with stirring. The resulting supernatant was dialyzed against 20mM HEPES, 0.1 mM PMSF, 10mM 2-mercaptoethanole, pH 7.0, loaded onto a HiTrap Blue HP Column (Amersham Biosciences) and eluted using a 0 – 1.0 M KCl_2 gradient. The peak fraction was dialyzed against 20mM HEPES, with the same additions, and loaded onto a Poros HS column (Applied Biosystems) and eluted with a 0.1 – 1.0 M KCl gradient. Purified F37I mutant was concentrated using an Amicon Ultra membrane and stored at −20°C in 50% Glycerol.

Assays and Michaelis-Menten kinetics

PPi-exchange assays were done at 37°C and initiated with 10 μl of enzyme to 190 μl of assay mix: 0.1M Tris-Cl, 0.01M KF, 5mM $MgCl_2$, 2mM ATP, 2mM Tryptophan, 70 mM 2-mercaptoethanol pH 8.0 plus 2mM ^{32}PPi at a specific radioactivity between 1×10^5 and 2×10^5 CPM/μM. Varying enzyme concentrations (4–400 μM) and incubation times (10–90 minutes) were used, depending on the activity level. Michaelis-Menten kinetics were examined by varying the [ATP] (0.01, 0.1, 0.3, 0.5, 1.0, 1.5, 2.0 mM). All assays were processed by eluting ^{32}P-ATP from charcoal with pyridine as described (Pham et al., 2006). For metal substitution assays the mix was made without Mg^{2+} and treated with Chelex 100 for 30 min at 4°C to remove the trace metals and supplemented with 10mM $MnCl_2$.

Protein design

Rosetta design was provided with structures (1D2RA, 1MAU, 1I6L) and a list of side chains required for catalytic activity, which were not to be mutated. Redesign cycles were carried out in which residues permitted to change were allowed to mutate and the mutant proteins were evaluated for stability using the empirical energy function(Dantas et al., 2003).

Graphics programs

Molecular illustrations were prepared using MACPyMOL (Delano, 2002). Graphs and line drawings were prepared with Kaleidagraph (Synergy, 2005) and CANVAS (Deneba, 200).

Acknowledgments

This work was supported by NIGMS-48519. We gratefully acknowledge substantive discussions with J. Hermans, A. Tropsha, P. Hansia, and H. Hu. We thank Eric First for suggesting the potential value of mutant/metal thermodynamic cycles, and G. Bricogne for pointing out the significance of molecular size for precision in catalysis.

References

Bandyopadhyay, D. A Geometric Framework for Robust Nearest Neighbor Analysis of Protein Structure and Function., Ph.D. University of North Carolina; Chapel Hill: 2005.

Bullock T, Uter N, Nissan TA, Perona JJ. Discrimination against glutamate by glutaminyl-tRNA synthetase. 2002In preparation

Burley SK, Petsko GA. Aromatic-Aromatic Interaction: A Mechanism of Protein Structure Stabilization. Science 1985;229:23–28. [PubMed: 3892686]

Carter, CW., Jr; Ilyin, VA.; Yin, Y.; Huang, X.; Retailleau, P. Three TrpRS Conformations Stabilize a Dynamic, Dissociative Transition State. Paper presented at: Using Crystallography to Understand Enzyme Mechanism; St. Paul, MN: American Crystallographic Association; 2002.

Carter, CW, Jr. Tryptophanyl-tRNA Synthetases. In: Cusack, S., editor. The Aminoacyl-tRNA Synthetases. Georgetown, TX: Landes Biosciences/Eurekah.com; 2005. p. 99-110.

Carter CW Jr, LeFebvre BC, Cammer SA, Tropsha A, Edgell MH. Four-body potentials reveal protein-specific correlations to stability changes caused by hydrophobic core mutations. J Mol Biol 2001;311:625–638. [PubMed: 11518520]

Cusack S, Tukalo M, Yaremchuk A. Class I tyrosyl-tRNA synthetase has a class II mode of cognate tRNA recognition. 2002In preparation

Dantas G, Kuhlman B, Callender D, Wong M, Baker D. A Large Scale Test of Computational Protein Design: Folding and Stability of Nine Completely Redesigned Globular Proteins. J Mol Biol 2003;332:449–460. [PubMed: 12948494]

Delagoutte B, Moras D, Cavarelli J. tRNA aminoacylation by arginyl-tRNA synthetase: induced conformations during substrates binding. EMBO J 2000;19:5599–5610. [PubMed: 11060012]

Delano, WL. The PYMOL Molecular Graphics System. San Carlos, CA: Delano Scientific; 2002.

Deneba. CANVAS. Victoria, British Columbia, Canada: ACD Systems International; 200.

Doublie S, Bricogne G, Gilmore C, Carter CW Jr. Tryptophanyl-tRNA synthetase crystal structure reveals an unexpected homology to tyrosyl-tRNA synthetase. Structure 1995;3:17–31. [PubMed: 7743129]

Fersht, A. Dissection Of The Structure And Activity Of An Enzyme. In: Kaiser, ET., editor. Design of Enzymes and Enzyme Models. Houston, TX: Robert A. Welch Foundation; 1988. p. 159-182.

Fersht AR. Dissection of the structure and activity of the tyrosyl-tRNA synthetase by site-directed mutagenesis. Biochem 1987;26:8031–8037. [PubMed: 3442641]

Fersht AR, Knill Jones JW, Bedouelle H, Winter G. Reconstruction by site-directed mutagenesis of the transition state for the activation of tyrosine by the tyrosyl-tRNA synthetase: a mobile loop envelopes the transition state in an induced-fit mechanism. Biochem 1988;27:1581–1587. [PubMed: 3284584]

First EA, Fersht AR. Mutation of Lysine 233 to Alanine Introduces Positive Cooperativity into Tyrosyl-tRNA Synthetase. Biochem 1993a;32

First EA, Fersht AR. Mutational and Kinetic Analysis of a Mobile Loop in Tyrosyl-tRNA Synthetase. Biochem 1993b;32:13658–13663. [PubMed: 8257699]

First EA, Fersht AR. Analysis of the role of the KMSKS loop in the catalytic mechanism of the tyrosyl-tRNA synthetase using multimutant cycles. Biochem 1995;34:5030–5043. [PubMed: 7711024]

Horovitz A, Fersht AR. Strategy for Analyzing the Co-operativity of Intramolecular Interactions in Peptides and Proteins. J Mol Biol 1990;214:613–617. [PubMed: 2388258]

Ilyin VA, Temple B, Hu M, Li G, Yin Y, Vachette P, Carter CW Jr. 2.9 A crystal structure of ligand-free tryptophanyl-tRNA synthetase: domain movements fragment the adenine nucleotide binding site. Protein Sci 2000;9:218–231. [PubMed: 10716174]

Kapustina M, Carter CW Jr. Computational Studies of Tryptophanyl-tRNA Synthetase: Activation of ATP by Induced-Fit. J Mol Biol 2006;362:1159–1180. [PubMed: 16949606]

Kapustina M, Hermans J, Carter CW Jr. Potential of mean force estimation of the relative magnitude of the effect of errors in molecular mechanics approximations. J Mol Biol 2006;362:1177–1180.

Krebs WG, Tsai J, Alexandrov V, Junker J, Jansen R, Gerstein M. Tools and Databases to Analyze Protein Flexibility: Approaches to Mapping Implied Features onto Sequences. Meth Enz 2003;374:544–584.

Mann, G.; Yun, RH.; Nyland, L.; Prins, J.; Board, JA.; Hermans, J., editors. The Sigma MD program and a generic interface applicable to multi-functional programs with complex, hierarchical command structure. New York: Springer Verlag, Berlin; 2002.

Marvin JS, Hellinga H. Manipulation of ligand binding affinity by exploitation of conformational coupling. Nat Struct Biol 2001;8:795–798. [PubMed: 11524684]

McGaughey G, Gagné M, Rappé AK. p-Stacking Interactions. J Biol Chem 1998;273:15458–15463. [PubMed: 9624131]

Pham Y, Li L, Kim A, Weinreb V, Butterfosss G, Kuhlman B, Carter CW Jr. A Minimal TrpRS Catalytic Domain Supports Sense/Antisense Ancestry of Class I and II Aminoacyl-tRNA Synthetases. Mol Cell 2006;25:851–862. [PubMed: 17386262]

Retailleau P, Huang X, Yin Y, Hu M, Weinreb V, Vachette P, Vonrhein C, Bricogne G, Roversi P, Ilyin V, Carter CW Jr. Interconversion of ATP binding and conformational free energies by Tryptophanyl-tRNA Synthetase: structures of ATP bound to open and closed, pre-transition conformations. J Mol Biol 2003;325:39–63. [PubMed: 12473451]

Retailleau P, Weinreb V, Hu M, Carter CW Jr. Crystal Structure of Tryptophanyl-tRNA Synthetase Complexed with Adenosine-5′ tetraphosphate: Evidence for Dissociative Character in the Transition State for Amino Acid Activation by Class I Aminoacyl-tRNA Synthetases. J Mol Biol 2007;369:108–128. [PubMed: 17428498]

Retailleau P, Yin Y, Hu M, Roach J, Bricogne G, Vonrhein C, Roversi P, Blanc E, Sweet RM, Carter CW Jr. High-resolution experimental phases for tryptophanyl-tRNA synthetase (TrpRS) complexed with tryptophanyl-5′AMP. Acta Cryst 2001;57:1595–1608.

SAS (2004). JMP (Cary, NC, SAS).

Sekine, S-i; Nureki, O.; Dubois, DY.; Bernier, S.; Chênevert, R.; LaPointe, J.; Vassylyev, DG.; Yokoyama, S. ATP Binding by glutamyl-tRNA synthetase is switched to the productive mode by tRNA binding. EMBO Journal 2003a;22:676–688. [PubMed: 12554668]

Sekine, S-i; Nureki, O.; Vassylyev, DG.; Bernier, S.; Chênevert, R.; LaPointe, J.; Yokoyama, S. Structural Basis for the tRNA-dependent Catalytic Activation of Glutamyl-tRNA Synthetase. EMBO Journal 2003b;22:676–688. [PubMed: 12554668]

Sekine, S-i; Shimada, A.; Nureki, O.; Cavarelli, J.; Moras, D.; Vassylyev, DG.; Yokoyama, S. Crucial Role of the HIGH-loop Lysine for the Catalytic Activity of Arginyl-tRNA Synthetase. J Biol Chem 2001;276:3723–3726. [PubMed: 11106639]

Sherlin LD, Perona JJ. tRNA-dependent active site assembly in a class I aminoacyl-tRNA synthetase. Structure . 2003In press

Sherman DB, Xhang S, Pitner JB, Tropsha A. Evaluation of the Relative Stability of Liganded Versus Ligand-Free Protein Conformations Using Simplicial Neighborhood Analysis of Protein Packing (SNAPP) Method. PROTEINS: Struct Funct Bioinform 2004;56:828–838.

Shimaoka M, Shifmann JM, Jing H, Takagi J, Mayo SL, Springer TA. Computational design of an integrin I domain stabilized in the open high affinity conformation. Nat Struct Biol 2000;7:674. [PubMed: 10932253]

Synergy. KaleidaGraph. Reading, PA: Synergy Software; 2005.

Tropsha A, Carter CW Jr, Cammer S, Vaisman II. Simplicial Neighborhood Analysis of Protein Packing (SNAPP): A Computational Geometry Approach to Studying Proteins. Meth Enz 2003;374:509–544.

Weinreb V, Carter CW Jr. Mg^{2+}-free *B. stearothermophilus* Tryptophanyl-tRNA Synthetase Activates Tryptophan With a Major Fraction of the Overall Rate Enhancement. J Am Chem Soc . 2007Under review

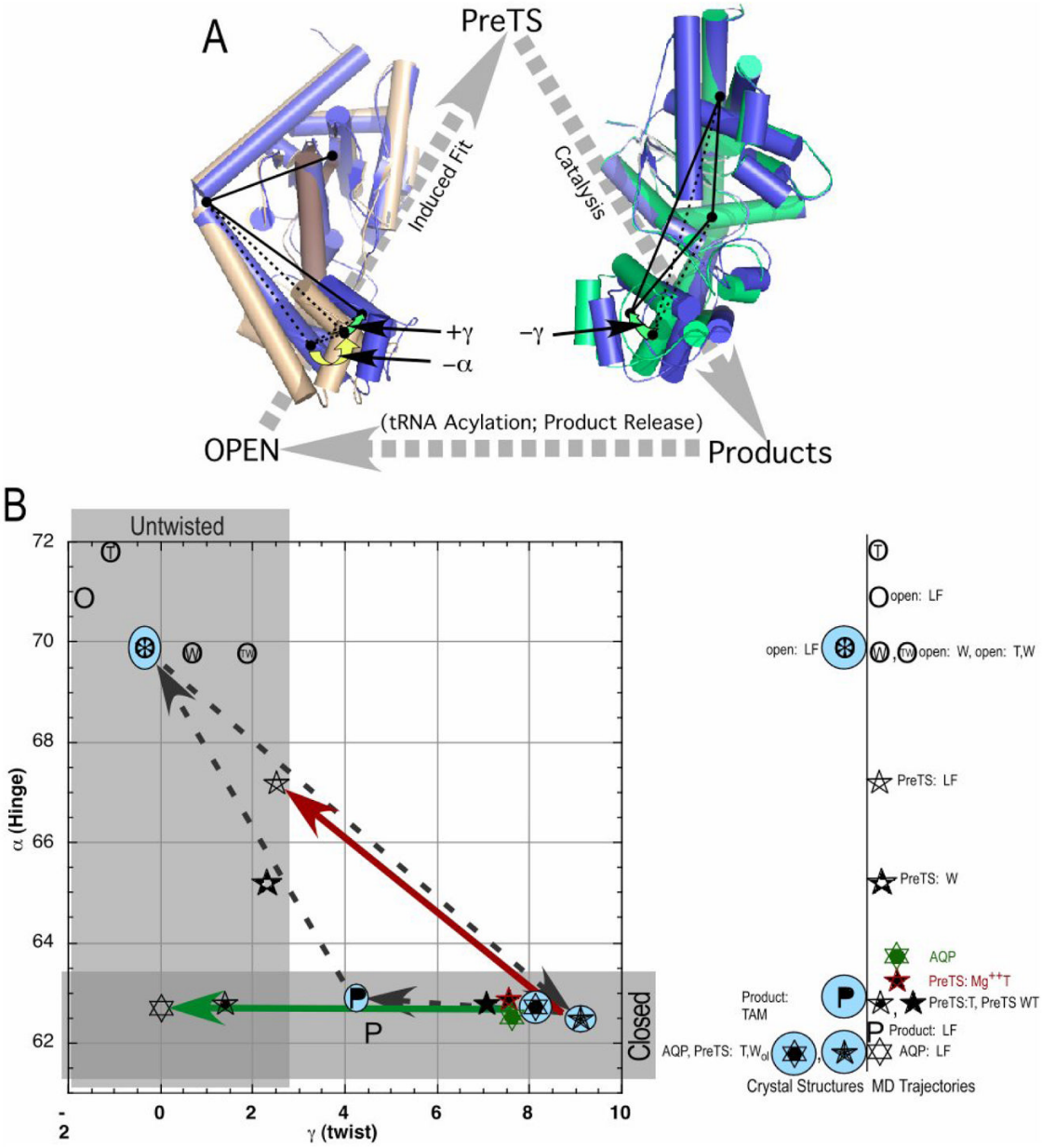

Figure 1.

TrpRS conformation space, spanned by interdomain angles, α (hinge-bending) and γ, (twisting). (A) Schematic diagram of changes between the three successive allosteric states (OPEN, wheat; PreTS, blue; Products, green) identified from crystal structures and connected by induced fit, catalysis, and product release (grey dashed arrows). Domain motions are described by two angles, hinge (α, yellow arrow) and twist (γ, green arrows). (B) Graphic summary of crystallographic and MD data. Dashed lines denote the structural reaction profile provided by the ensemble of X-ray crystal structures, represented by symbols surrounded by blue ellipses. Other symbols represent endpoints of 5 ns MD trajectories. Colored arrows denote trajectories described in this work. Initiated from the respective crystallographic coordinates in the absence of ligands, they define a conformational transition state between the PreTS complexes (red) and the AQP complex (green).

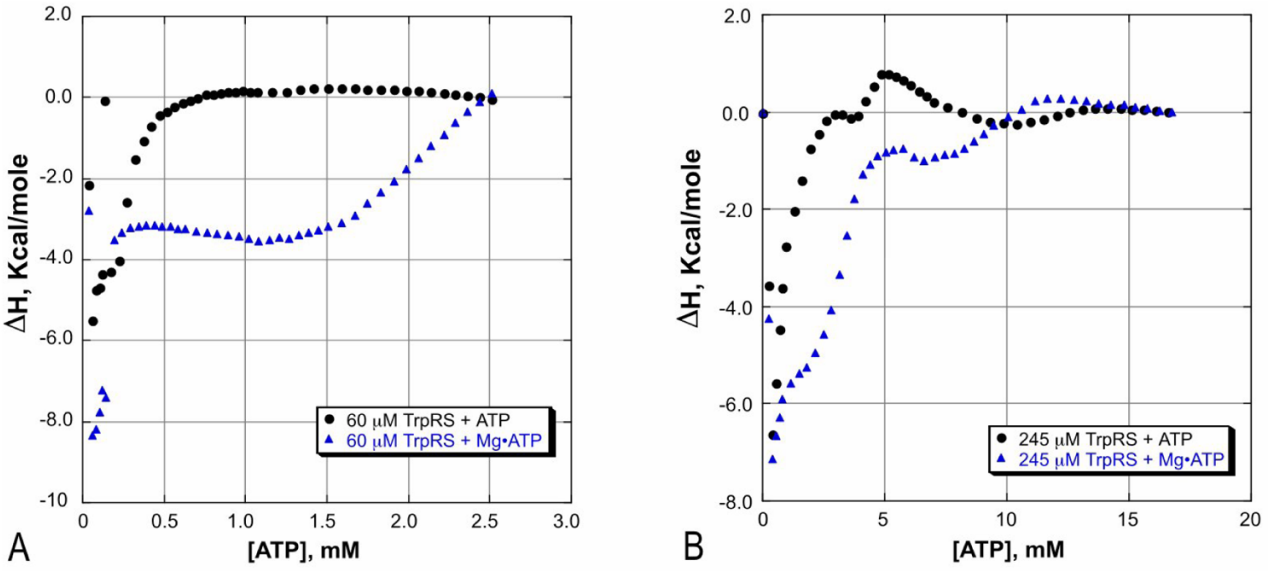

Figure 2.

ITC analysis of the effect of Mg^{2+} on TrpRS•ATP affinity. (A) Titration of 60 μM TrpRS with additions of 15 mM ATP. (B) Titration of 245 μM TrpRS with additions of 0.1 M ATP. Curves with and without Mg^{2+} have similar shape, but are displaced relative to one another, consistent with the conclusion that Mg^{2+} weakens ATP binding to TrpRS.

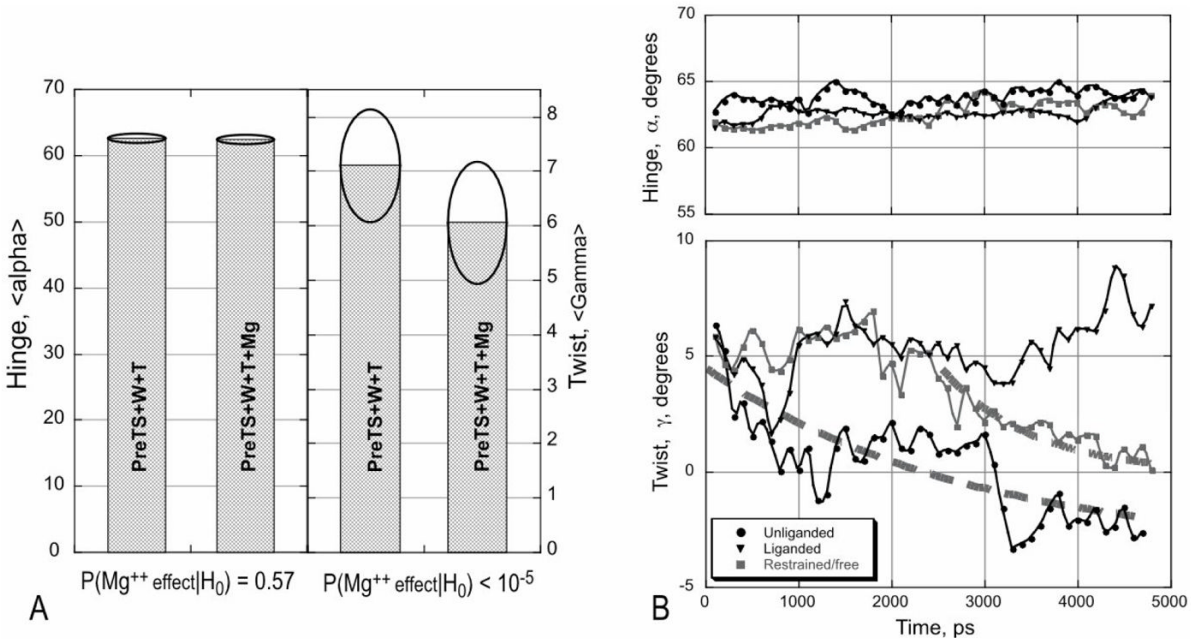

Figure 3.

PreTS and AQP trajectories. (A) Unrestrained Mg^{2+} ion destabilizes the high twist angle even in fully liganded PreTS TrpRS with Trp and ATP. The hinge angle remains constant in both simulations. Introducing Mg^{2+} ion leads to a smaller twist angle. Ellipses indicate the range of values. (B) Trajectories for liganded and domain-restrained unliganded AQP complexes both retain a conformation close to that of the crystal structure, while the unliganded form progresses rapidly toward and beyond the product state. Removing the forcing potential (2500 ps) from the restrained trajectory leads to rapid loss of the high twist angle. Dashed gray lines fit a single exponential to the data points for the decaying parts of the unliganded trajectories.

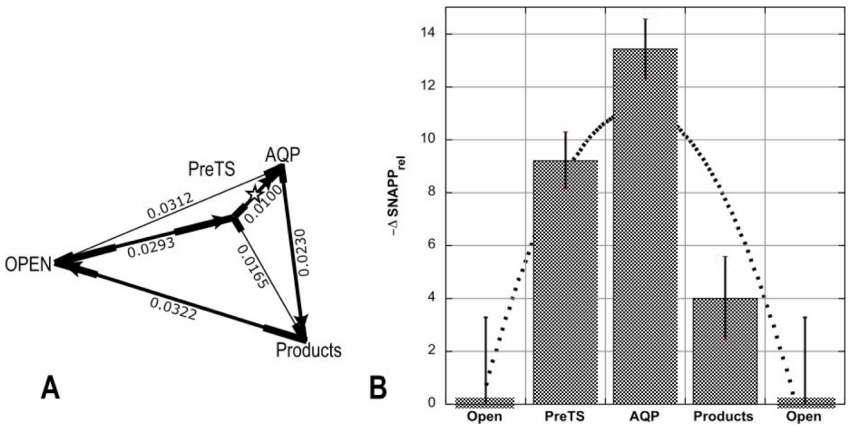

Figure 4.

ΔSNAPP analysis of the conformational cycle. (A). Distances, d = 1−R, are calculated between the four distinct structural clusters from the cross correlation coefficients, R. Thick lines denote the presumptive reaction coordinate passing through the structures, and the star denotes the conformational transition state. Broad lines at each vertex represent standard deviations evaluated from those of the self- and cross-correlations. The four groups of structures are significantly different from one another. (B) ΔSNAPP values calculated relative to that of the Open structures, with standard deviations. The ordinate, -ΔSNAPP, reflects unfavorable statistical free energy changes. The dashed line is a least squares fit to a parabola.

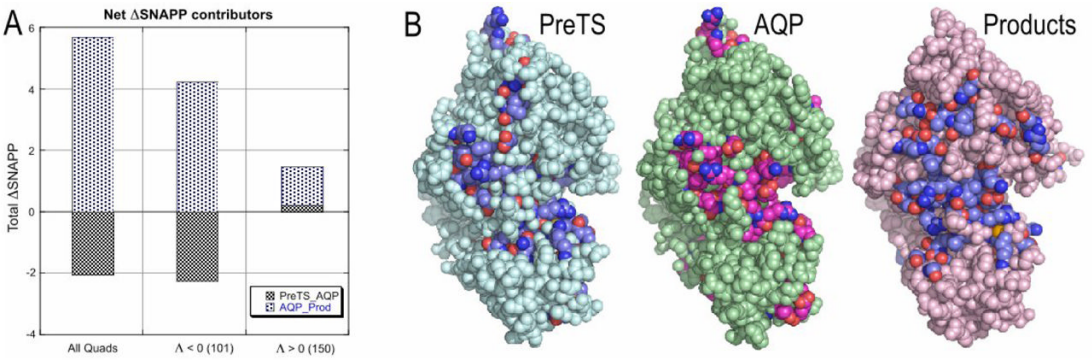

Figure 5.

Contributions of tertiary positive- and negative-Λ Delaunay tetrahedra to the overall ΔSNAPP values in Figure 4B. A. Total ΔSNAPP values for the two transitions, PreTS=>AQP (grey) and AQP=> Product (blue) relevant to the catalytic step are shown in the left-hand panel. Individual ΔSNAPP were evaluated and summed for all ~250 tetrahedra. Of these, ~100 have Λ< 0 (middle) and ~150 have Λ > 0 (right). The total ΔSNAPP values result largely from the former set. B. Spatial arrangement of negative-Λ tetrahedra in PreTS, AQP, and Products structures.

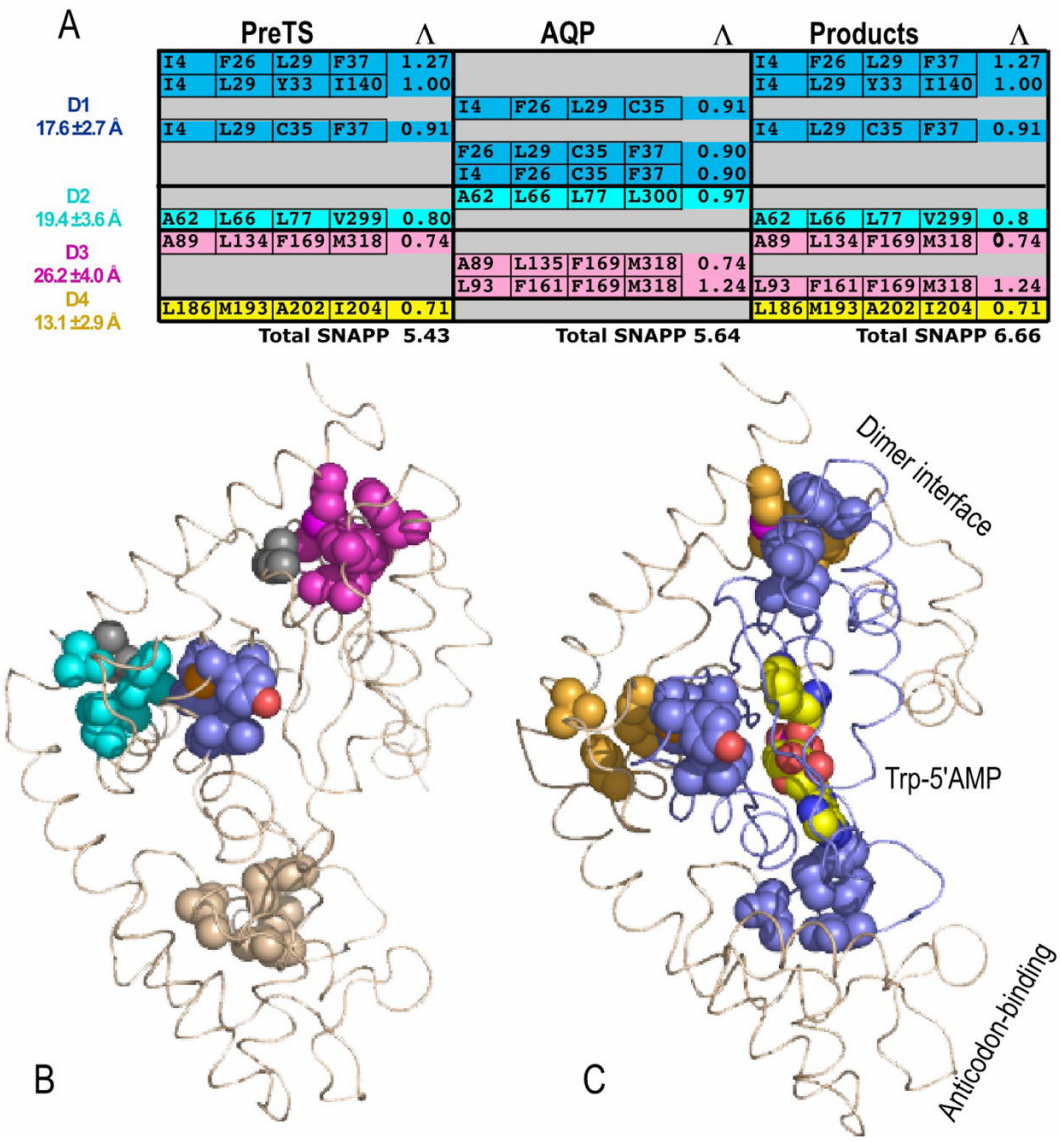

Figure 6.

Localized side chain packing changes associated with passage through the conformational transition state. (A) High-Λ Delaunay tetrahedra that change composition. Colors correlate with the locations of four clusters in (B). (B) The four clusters indicated in (A). Grey spheres represent alternate partners encountered in the AQP state. (C) Distribution of the components of the tetrahedra in (A) between the MCD (slate) and the remaining mass of the protein (wheat), and their relationship to Trp-5′AMP (yellow). Switching interactions D3 and D4 mediate communication to the dimer interface and anticodon-binding domain, respectively.

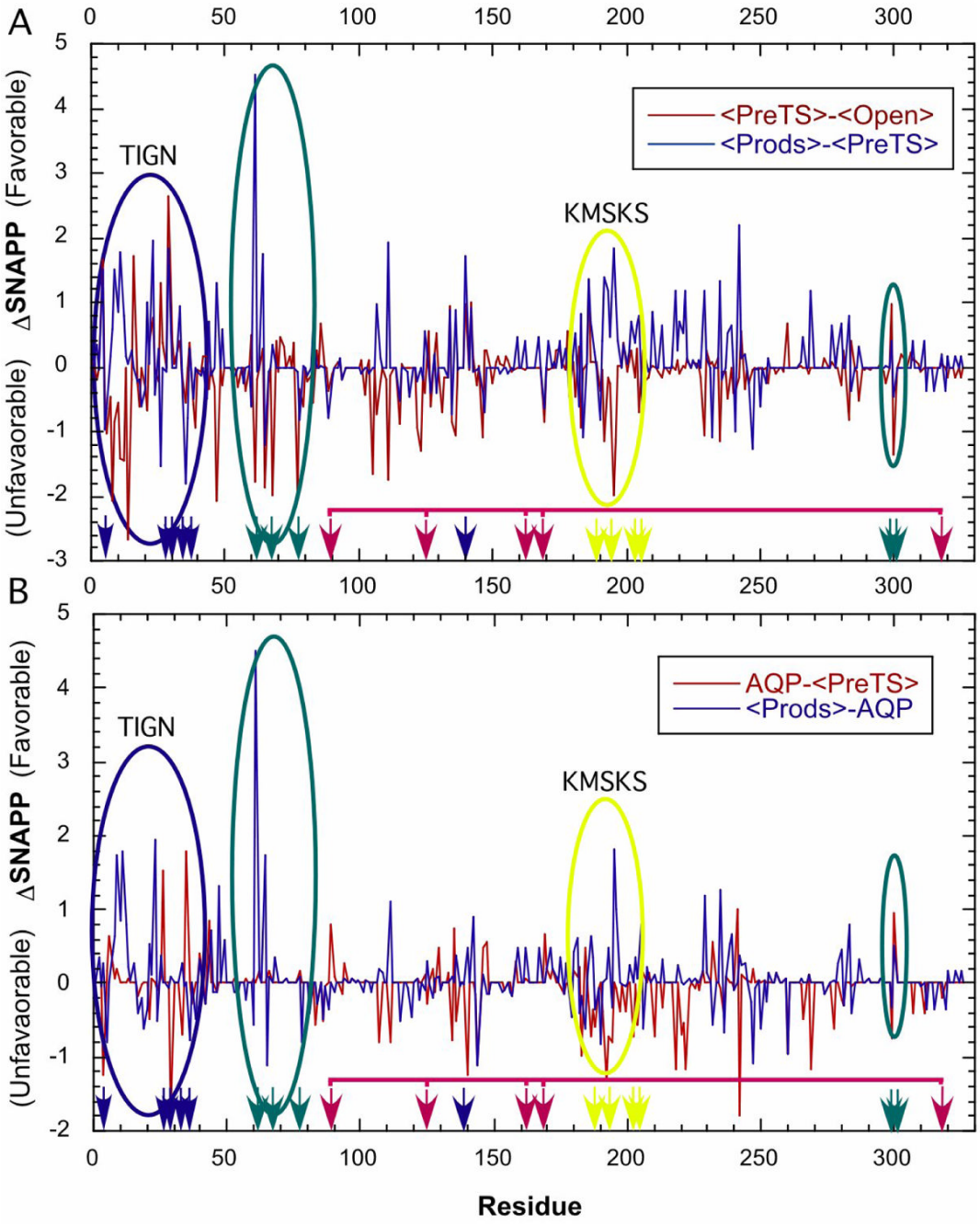

Figure 7.

Residue-by-residue ΔSNAPP analysis of the conformational cycle for amino acid activation by TrpRS. Favorable changes on the ordinate are positive. The four groups of residues illustrated in Figure 6 are indicated by colored arrows. Three are highlighted by colored ellipses. Two, involving the TIGN (blue) and KMSKS (yellow) sequences, are local. The other two, including the domain hinge region (green) and one close to the dimer interface (red) are distributed throughout the sequence. (A) The overall transition from PreTS to product. (B) Conversions to and from the AQP state, which most resembles the conformational transition state.

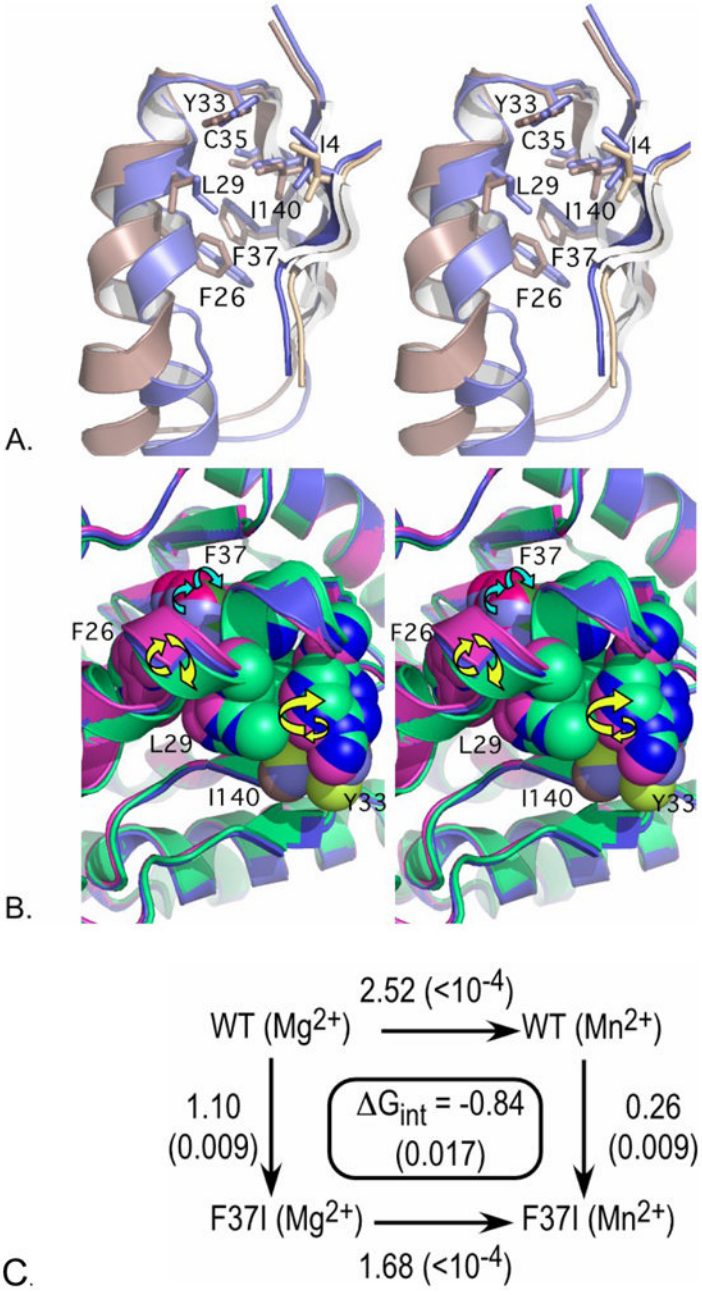

Figure 8.

Catalytic involvement of the TrpRS D1 cluster. (A) Rearrangement of the D1 cluster during induced fit assembly of the open form (wheat) to the PreTS state (slate). The N-terminal α-helix closes against the parallel β-sheet, causing F26 to stack against F37. (B) Changes during catalysis, PreTS=>AQP=>Products, are more subtle. The C-terminus of the αA helix shortens (AQP, magenta), then lengthens (Products, green) from its configuration in the PreTS state (blue). Nearest neighbor repacking in the first step is retrograde (yellow arrows) for most side chains, as shown by the banding of colors in Y33, while it is progressive for F37 (cyan arrows). (C) The F37I/Mn^{2+} double variant thermodynamic cycle. Δ ($\Delta G^{\ddagger}_{kcat}$) values (kcal/mole) for each effect, with t-test probabilities in parentheses. R^2 for the regression model is 0.98.

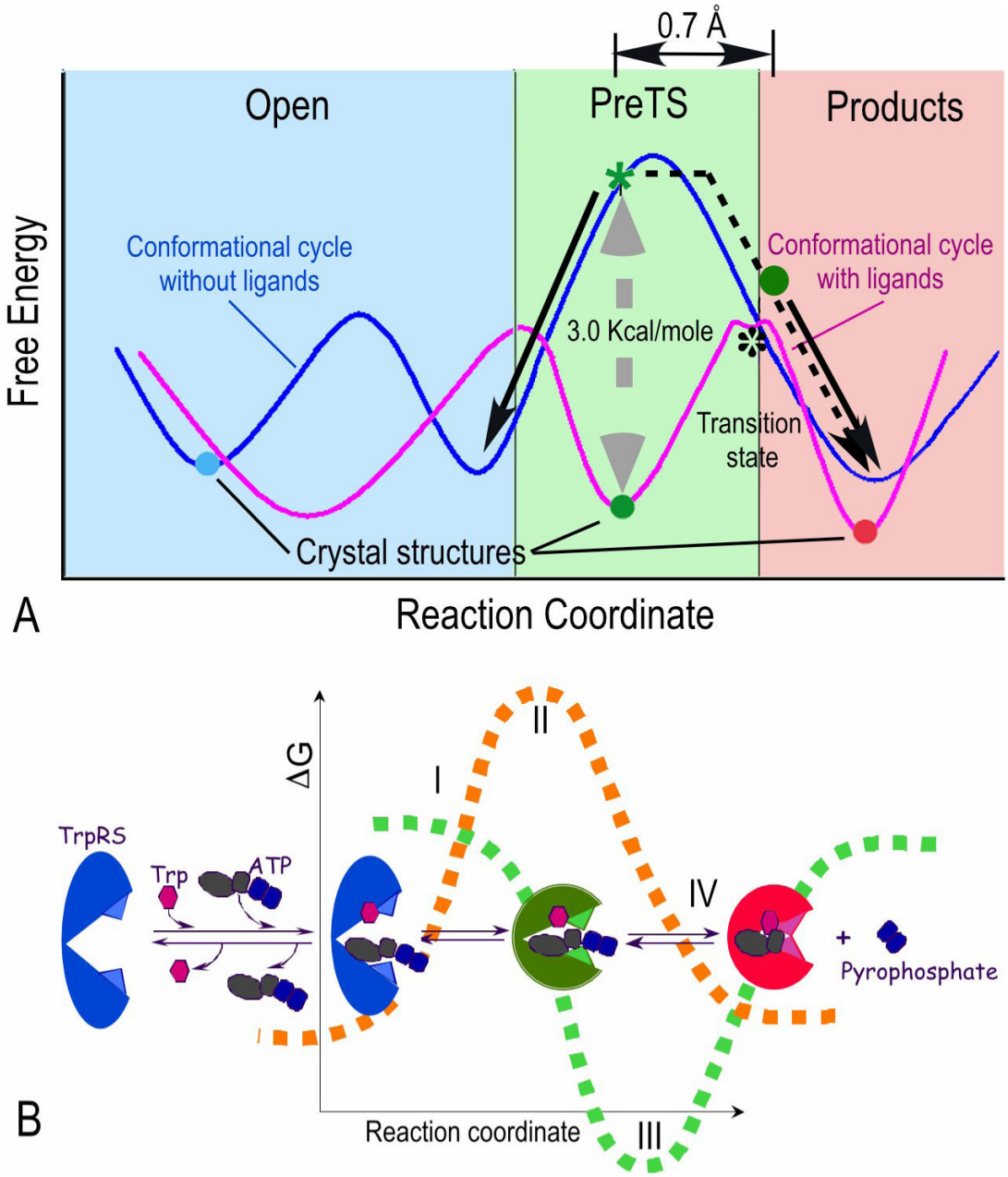

Figure 9.

Conformational free energies and catalysis of tryptophan activation by *B. stearothermophilus* TrpRS. (A) Schematic of conformational free energy along the reaction coordinate. The experimentally determined free energy difference between ATP-bound (magenta line) and unliganded (blue line) PreTS conformations (grey dashed arrow) represents the free energy stored during induced fit. (B) Catalytic effects produced by conformational and binding free energy curves. (I) Induced fit. The unfavorable twist angle allows lysine residues, K111, K192, and K195 to weaken interactions of ATP phosphate groups with the catalytic Mg^{2+} ion and destabilize the ground state. (II) Conformational switching interactions pose a (small) barrier to the progression to products. (III) The adenosine and PPi binding subsites

move significantly apart as high transition state binding affinity (green, dashed curve) is realized. (IV) Conformational free energy is recovered (orange, dashed curve).